

Regularized Quadrature Filters for Local Frequency Estimation: Application to Multimodal Volume Image Registration

Jundong Liu

Dept. of CISE, University of Florida
Gainesville, FL, 32603
USA
Email: jliu@cise.ufl.edu

Abstract

Multimodal image registration is a fundamental problem in medical image analysis. In this paper, we propose a novel algorithm to compute the local frequency representations of the multimodal data sets to be registered. Local frequency representation can detect edge and ridge information simultaneously. In this algorithm, we develop regularized quadrature filters (RQFs) to compute local frequency maps, which are relatively insensitive to noise in comparison to standard QFs. The local frequency maps thus obtained are used as an underlying representation to which a statistically robust matching technique is applied, to estimate a parameterized transformation between the volume data sets. We present experimental results for registering several pairs of CT-MR data sets along with comparisons to other matching methods.

1 Introduction

Image registration is one of the most widely encountered problems in a variety of fields including but not limited to medical image analysis, remote sensing, satellite imaging, optical imaging etc. Broadly speaking, image registration methods can be classified into two classes [18] namely, feature-based and direct methods. In the former, features are extracted from the two images to be registered and matched to estimate the transformation between the two data sets. In the latter, the coordinate transformations between the images are determined directly from the image data or a derived image-like representation of the same.

1.1 Feature-based Methods

In [7], Evans *et al.* developed a registration scheme based on approximating the 3D warp between the model and target image by a thin plate spline fitted to landmarks. Davatzikos *et al.* [6] introduced a two stage brain image registration algorithm. The first stage involved using active contours to establish a one-to-one mapping between cortical and ventricular boundaries in the brain and in the second stage, an elastic deformation that determines the best correspondence between the identified contours in the two data sets is determined. Feldmar *et al.*, [8] developed a novel surface to surface nonrigid registration scheme, using a local affine transformation. For more on feature-based methods, we refer the reader to the survey by Maintz *et al.*, [12]. *All of these approaches have one commonality, i.e., they need to detect features/surfaces/contours in the images and hence the accuracy of registration is dictated by the accuracy of the feature detector.*

1.2 Direct Methods

The most popular direct approach is based on the concept of maximizing mutual information reported in Viola and Wells [20], Collignon *et al.*, [5] and Studholme *et al.*, [17]. Mutual information between the source and the target images that are to be registered is maximized using a stochastic analog of the gradient descent method in [20] and other optimization methods such as the Powell's method in [5] and a multiresolution scheme in [17]. Reported registration experiments in these works are quite impressive for the case of rigid motion. Most mutual information based algorithms in literature have been formulated for global parameterized motion with the exception of the recent work reported in Meyer *et al.*,

[15] wherein affine transformations as well as thin-plate spline warps are handled. The reported registration results are quite impressive but the CPU execution times are quite high – of the order of several hours for estimating thin-plate warps.

1.3 Overview of the Proposed Registration Method

In this paper, we develop a multi-modal registration technique which is based on a *local frequency* representation of the image data. A *local frequency* image representation is obtained by filtering the image with a *quadrature filter* (QF) tuned to a certain frequency/orientation and then computing the gradient of the phase of the filtered image. *local frequency representation is relatively invariant to changes in illumination conditions which cause gray value changes.* What does this mean in the context of multi-modal registration? Because, multi-modal images of the same underlying object have completely different intensities, a local frequency-based representation seems apt to capture the salient common features between the two modalities. *This is the premise underlying the development of our multi-modal registration algorithm to be described subsequently.* We will use examples to show how local frequency can be used to capture high frequency features, like edge and ridge simultaneously. It should be noted that noise also has high frequency components, and standard QFs, e.g. Gabor filter, are quite sensitive to the existence of noise. A robust QF is needed to suppress the effect of noise and make the resulted image representation more faithful in describing meaningful features. we present a regularized QF and show its superiority over the standard QFs in term of dealing with noise.

Once we compute this local frequency representation for each of the two (source and target) images to be registered, we are ready to find the registration which will best match these representations. Several matching criteria may be defined; we use a robust measure based on the integral of the squared error (ISE or L_2E) between a Gaussian model of the residuals and their true density function [16]. The residuals here refer to the difference between the local frequency representations of the transformed (by an unknown transformation) source and target data. This robust estimation framework affords the

advantage of not having to deal with additional tuning parameters that would be required when using influence functions to achieve robustness. We minimize this L_2E matching criteria over all rigid/affine transformations using a preconditioned gradient descent technique. We present results of applying this algorithm to MR and CT images that are misaligned due to real motion of the patient during imaging. *One of the key strengths of our method is that – due to the formulation being set in a robust framework – it can handle data sets that do not have significant overlap as is the case in most practical situations.* Additionally, the formulation can be easily extended to handle non-rigid deformations by employing the level-set registration scheme described in Vemuri et.al., [19] in the local-frequency representation framework. This is the topic of our ongoing efforts.

2 Local Frequency Representation

For multimodal image registration, the relation between the brightness of the corresponding pixels is usually complicated: multiple intensity values in one modality image may map into single intensity in another modality; image feature existing in one image may not have correspondence in the other image [1], etc. In order to successfully solve the multimodal registration problem, two questions have to be answered: 1) what kind of common information should be extracted from the image pair? 2) how to reject outliers to ensure accuracy and robustness?

Tomes of research has been reported on retrieving information that is shared by the multi-modal data sets while reducing or eliminating the (imaging) sensor dependent background information. In [1], the authors presented an energy-image representation based on directional-derivative filters. Four directional derivative filters, oriented in the horizontal, vertical, and the two diagonal directions, are applied to the raw image. Thus The directional information is preserved in this energy representation.

Multi-modal image data, acquired either with different sensors, or with the same sensor but with different illumination conditions, mainly differ in the background of the image, or in other words, in the low frequency components. High frequency components, on the other hand, normally correspond to the physical structure of the sensor, and thus are good

at expressing the commonality existing within the multisensor image pair. In the local frequency representation on which our algorithm is based, edges and ridges will have high values (since they are associated with high frequency components) and will be the dominant features for the matching stage.

In order to define the local frequency representation, we will first introduce the concept of an analytic signal/function in 1D which can be generalized to higher dimensions [10]. Given a signal f in 1D, its analytic signal is defined as $f_A = f - if_{Hi}$, where f_{Hi} is the Hilbert transformation of f and given by $f_{Hi} = 1/\pi \int_{-\infty}^{+\infty} (f(\tau)/(\tau - x))d\tau$. The transformation from the real signal to its corresponding analytic signal can be regarded as the result of convolving the real signal with a complex filter, which is called a *quadrature filter*.

The argument of f_A is referred to as the *local phase* of f , which is defined in the spatial domain. The spatial derivative of local phase is called *local* or *instantaneous frequency* [10].

Given a signal f in 1D, its analytic signal is defined as $f_A = f - if_{Hi}$, where f_{Hi} is the Hilbert transformation of f . The argument of f_A is referred to as the *local phase* of f . The spatial derivative of local phase is called *local* or *instantaneous frequency* [10].

The following properties of local frequency make it a candidate for an invariant image representation in matching multi-modal image data set: (1) Local frequency estimate are relatively invariant to signal energy, in other words, also independent to the image contrast. This makes a notable advantage over ordinary gradient-based edge detector: some important features, e.g. ventricle in CT brain image, resides in a region with a quiet small contrast again background. Gradient methods will probably fail to detect them efficiently, while local frequency representation can do this work well. [10]. (2) Local frequency estimation can detect edge, ridge and texture information at the same time. This imposes an advantage over the methods use in [11], where the edge and ridge have to be extracted by different operators.

2.1 Gabor Filters

First we would like to present the local frequency estimation using Gabor filters, which are well-known QF's. They achieve the theoretical lower bound of the uncertainty principle [10] i.e., Ga-

bor functions are optimal in terms of their space-frequency localization. The complex 2-D Gabor functions have the following general form (see Bovik et.al. [4] for details on following definitions):

$$h(x, y) = g(x', y')exp(2\pi j(Ux + Vy)), \quad (1)$$

where $(j = \sqrt{-1})$, $(x', y')^T = R(x, y)$ with R being the 2D rotation matrix and

$$g(x, y) = \left(\frac{1}{2\pi\lambda\sigma^2} \right) exp \left(-\frac{\left(\frac{x}{\lambda}\right)^2 + y^2}{2\sigma^2} \right). \quad (2)$$

Therefore, $h(x, y)$ is a complex sinusoid modulated by a 2-D Gaussian function whose aspect is given by λ , scale parameter by σ , and the major axis making an angle ϕ with the x-axis. For $\lambda = 1$, $g(x, y)$ is circularly symmetric and hence ϕ need not be specified. The frequency response of the Gabor function in eqn. 1 is given by

$$H(u, v) = exp\{-2\pi^2\sigma^2[(u' - U')^2\lambda^2 + (v' - V')^2]\} \quad (3)$$

where $(u', v') = (ucos\phi + vsin\phi, -usin\phi + vcos\phi)$ and (U', V') is a similar rotation of the central frequency (U, V) . Hence, $H(u, v)$ happens to be a Gaussian bandpass filter with its minor axis at an angle ϕ from the u-axis, an aspect parameter of $1/\lambda$, a radial central frequency $\Lambda = \sqrt{(U^2 + V^2)}$ and orientation $\theta = \tan^{-1}(V/U)$ with respect to the u -axis.

2.2 Computing local-frequency representation

The process of computing the local frequency representation can be achieved in three steps:

For each tuning frequency (ω, θ) do:

- generate a Gabor filter $G(x, y)$ tuned to direction θ and frequency ω , and let $q_+(x, y)$ and $q_-(x, y)$ be the result of convolution of the image I with the real and imaginary parts of G respectively.
- Compute the local phase gradient (local frequency estimator) for each filter using the following equation:

$$\nabla\phi(x, y) = [q_+(x, y)*\nabla q_-(x, y) - q_-(x, y)*\nabla q_+(x, y)]/[q_+^2(x, y) + q_-^2(x, y)] \quad (4)$$

where $\phi(x, y) = arctan(q_-(x, y)/q_+(x, y))$ (note that ϕ needs not be explicitly computed)

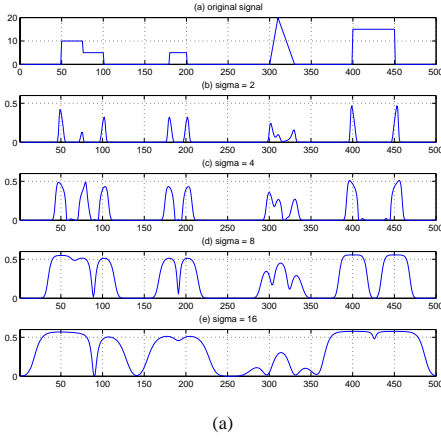


Figure 1: (a) original 1D signal; (b)-(e) Local frequency estimations with different scaled gabor filters (σ increases from 2 (in b) to 16 (in e))

- Construct an image representation (the average squared local frequency magnitude) by summing squared gradient magnitudes for each filter as follows:

$$F(x, y) = \sum_{\omega} \sum_{\theta} |\nabla \phi(x, y)|^2 \quad (5)$$

Figure 1 shows a local frequency estimation with different scaled gabor filters. Fig1.a is the original one dimensional signal. It contains both edges and ridges with different contrasts. Fig1.b - 1.e are local frequency estimations with different scaled gabor filters. The filter bank have the same tuning frequency, but differ in the scale parameter σ , which increases from 2 (b) to 16 (e).

As we can see, the local frequency outputs construct a multi-scale representations for edge and ridge detection. Two noticeable characteristics are demonstrated in this experiment: (1) the local frequency, unlike gradient, relatively independent to signal contrast; (2) the localization of the detector is quiet faithful to the original signal. The latter property is due to the stability of phase information [9].

The scale space properties of local frequency estimation, as shown in Fig.1 have long been exploited in the computer vision community both from a computational and localization of features point of view. Using scale-space i.e., multi-resolution processing leads to computationally efficient algorithms and alleviates the problem of local-minima entrapment when used in the context of

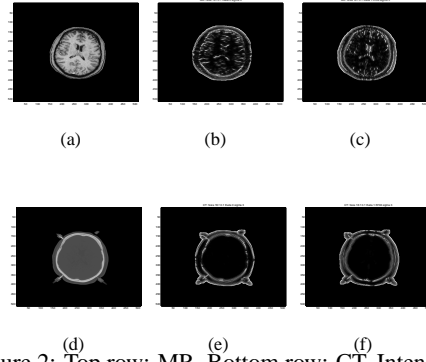


Figure 2: Top row: MR; Bottom row: CT. Intensity image (left column) and two local frequency images generated using Gabor filters with $\theta = 0$ (middle column) and $\theta = \pi/2$ (right column)

non-convex function optimization e.g., the registration problem described in the next section.

Figure 2 depicts a pair of MR-CT slices and the associated local frequency representations. obtained by applying the oriented (in two directions) Gabor filters.

3 Regularized Quadrature Filters

By combining two well-known topics in signal processing: quadrature filters and Bayesian estimation with Markov random fields (MRF's) as prior models, Marrouquin et.al [14] present a class of robust QFs which have a built-in smoothing property to deal with missing observations and noise.

Bayesian estimation has been widely used to solve ill-posed problems that frequently arise in signal processing and computer vision. Many of these problems have the following form:

Find a smooth function f defined on the nodes of a regular lattice L , given observations g that may be modeled by

$$g(x) = Af(x) + n(x), x \in S. \quad (6)$$

A regularized solution to this kind of ill-posed problems can be defined as the minimizer of a functional of the form

$$U(f) = \sum_{x \in S} \phi_{f,g}(x) + \lambda \sum_C V_C(f) \quad (7)$$

where $\phi_{f,g}$ is a function that in general depends on the noise model; V_C is the potential function associated with a prior Markov random field model,

where C are the cliques of the corresponding neighborhood system. The parameter λ depends on the noise variance.

A particularly important case is where the f field is assumed *a priori* to be globally smooth. The most popular prior models is squares of first-order derivatives (membrane):

$$V_{ab}(f) = [f(a) - f(b)]^2 \quad (8)$$

and the second-order derivative (thin-plate):

$$V_{abc}(f) = [-f(a) + 2f(b) - f(c)]^2 \quad (9)$$

$$V_{pqrs}(f) = 2 [-f(p) + f(q) - f(r) + f(s)]^2 \quad (10)$$

where a, b, c and p, q, r, s are neighboring sites in one and two dimension respectively.

The minimizer of Eq.8 smoothes out the observation field g , interpolating over those sites where information is missing; hence the minimization operation may be considered as a robust low-pass filter acting on g . Using a first-order prior MRF model and setting the gradient of Eq.8 equal to zero, one obtains a set of linear equations of the form

$$f(x) + \lambda[-f(x-1) + 2f(x) - f(x+1)] = g(x) \quad (11)$$

. Taking the Fourier transform on both sides, one can get the transfer function of this low-pass filter

$$H(\omega) = \frac{1}{1 + 2\lambda(1 - \cos \omega)} \quad (12)$$

From this regularized low-pass filter, one can obtain a one-dimensional QF by shifting the frequency response to the desired tuning frequency: T

$$H(w) = \frac{1}{1 + 2\lambda(1 - \cos(\omega - \omega_0))} \quad (13)$$

The corresponding potential is:

$$V_{ab}(f) = |f(a) - f(b)e^{i\omega_0} \cdot (a - b)|^2$$

(note that now f is complex-valued). Similarly, the shifted and rescaled transfer function of a 'thin-plate' model with potential given by Eq. 9 is

$$H(w) = 1/[1 + \lambda\{6 + 2 \cos[2(\omega - \omega_0)] - 8 \cos(\omega - \omega_0)\}] \quad (14)$$

which entails a corresponding modification of the second order potentials. For higher dimension cases, the derivation procedure is similar. We refer readers to [14] for more details.

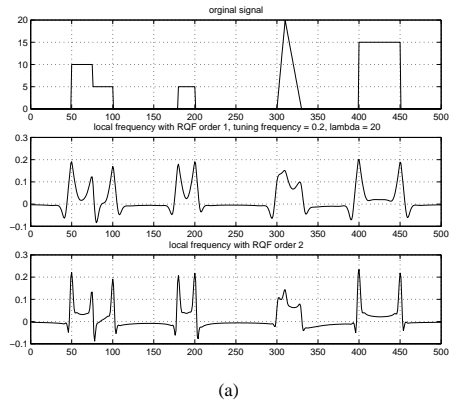


Figure 3: Top row: original 1D signal; Second row: local frequency estimation with first-order RQF; Third row: local frequency with second-order RQF.

3.1 Estimate Local Frequency with RQFs

The procedure of estimating local frequency using RQFs is identical with the steps presented in section 2.2 except that the Gabor filter should be replaced with RQFs.

Fig.3 illustrates the local frequency estimation with two RQFs. As we can see, the RQFs have the same property of Gabor in term of detecting edge and ridge. The spatial localization of edge is quiet accurate.

Fig.4 shows an example of the effect of noise on the local frequency estimation. Top row is the original noised 1D signal. Second row shows the local frequency output with Gabor filter, while third and fourth rows demonstrate the outputs from first-order and second-order RQFs respectively. As it is evident, both RQFs are better that Gabor in sense of maintaining relatively robust detection of edge and ridge. Figure 5 shows the one slice of MR/CT image pair, together with corresponding local frequency images estimated by using a second-order RQF.

4 Matching Local Frequency Representations

To match the local-frequency representations of the image pair, we develop a robust matching criteria based on minimization of the integral squared error (ISE) also known as the L_2 error or simply L_2E be-

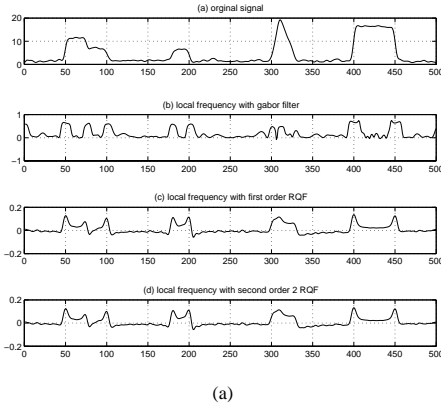


Figure 4: Top row: noised 1D signal; Second row: local frequency estimation with Gabor filter; Third row: with first-order RQF. bottom row: with second-order RQF.

tween a Gaussian model of the residual error and the true density function of the residual. Here the residual error refers to the difference between the transformed local frequency representation of the source image and the local frequency representation of the target image. It should be noted that the integral squared error has been very popular as a goodness-of-fit criteria in non-parametric density estimation. It was shown in Scott [16] that minimum distance estimators, including the L_2E , are inherently robust without requiring the need to specify any tuning parameters found in robust likelihood methods.

Let the local frequency representations of the CT-MR image pairs (or MR-MR pair acquired under different imaging protocols) differ by a local displacement, then, the following equation holds for the local-frequency representations:

$$F_1(\mathbf{X} + \mathbf{T}) = F_2(\mathbf{X}) + \epsilon(\mathbf{X}) \quad (15)$$

where the residual error field ϵ is assumed to be composed by independent, identically distributed random variables, $F_1(\cdot)$ and $F_2(\cdot)$ are the 3D local frequency image representations computed from the MR and CT data sets respectively, $\mathbf{X} = (x, y, z)$, $\mathbf{T} = (u, v, w)$ is the 3D displacement field at the (x, y, z) points. Our goal is to minimize the L_2E measure given by

$$\min_{\mathbf{T}} \mathcal{E}(\mathbf{T}) = \int \{g(\epsilon/\theta) - h(\epsilon)\}^2 d\epsilon \quad (16)$$

where $g(\cdot)$ is a Gaussian function modeling the density of the residual error, $\theta = [\mu, \sigma]$ being the vector

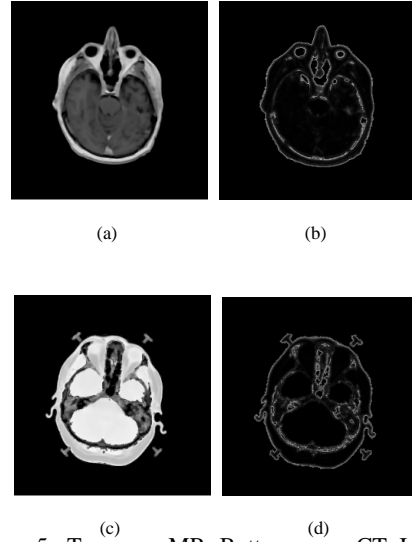


Figure 5: Top row: MR, Bottom row: CT. Intensity image (left column) and corresponding local frequency images (right column) generated using a second-order RQF.

describing the Gaussian density parameters μ and σ the mean and variance respectively, and h is the true unknown density of the residual error term. Expansion the integrand leads to two terms that are dependent on T and a third term $h^2(\cdot)$ independent of T , which can be ignored from the minimization. The first term in the expansion is $\int g^2(\cdot)$ and the second term is $-2E_h g(\cdot/\theta)$ the expectation of $g(\cdot)$ with respect to h , the true density of the residual. The first term being a Gaussian can be evaluated in closed form and we can use the following unbiased estimator for the second term,

$$-\frac{2}{N} \sum_{i=1}^N g(F_1(\mathbf{X}_i + \mathbf{T}_i) - F_2(\mathbf{X}_i)/\theta) \quad \text{for } i = 1, \dots, N \text{ lattice points.} \quad (17)$$

Thus, the minimization using the L_2E criterion is given by

$$\min_{\mathbf{T}, \mu, \sigma} \mathcal{E}(\mathbf{T}, \theta) = \frac{1}{2\sqrt{\pi}\sigma} - \frac{2}{N} \sum_{i=1}^N \exp\left\{-\frac{(F_1(\mathbf{X} + \mathbf{T}) - F_2(\mathbf{X}) - \mu)^2}{2\sigma^2}\right\} \quad (18)$$

In this paper we will limit the parameterized motion to 3D affine transformation, which is expressed with 12 unknown parameters to control rotation, translation and scaling. To estimate the transformation, we solve the minimization problem in equation 18 using a preconditioned gradient descent with successive step length reduction.

4.1 Numerical Implementation

The basic iterative form for a host of gradient-based numerical methods can be written down as

$$\mathbf{x}^{k+1} = \mathbf{x}^k - \alpha^k \mathbf{D}^k \nabla \mathcal{E}(\mathbf{x}^k) \quad (19)$$

where \mathcal{E} is the function being minimized and \mathbf{D}^k is a positive definite symmetric matrix, α^k is the step length and a condition to be observed in descent methods is $\nabla \mathcal{E}(\mathbf{x}^k)^t \mathbf{D}^k \nabla \mathcal{E}(\mathbf{x}^k) > 0$. This will hold since \mathbf{D}^k is positive definite. For the case of Steepest descent, $\mathbf{D}^k = \mathbf{I}$ for all k , for the Newton method, $\mathbf{D}^k = (\nabla^2 \mathcal{E}(\mathbf{x}^k))^{-1}$ for all k . We choose $\mathbf{D}^k = \text{diag}(d_1^k, d_2^k, \dots, d_n^k)$, where the notation $\text{diag}(\cdot)$ indicates a diagonal matrix. The step size α can be determined using line search which basically involves a minimization given by $\mathcal{E}(\mathbf{x}^k + \alpha^k \mathbf{d}^k) = \min_{\alpha \geq 0} \mathcal{E}(\mathbf{x}^k + \alpha^k \mathbf{d}^k)$. For reasons of computational efficiency, we choose successive step length reduction using the Armijo rule (see [3] for a discussion).

5 Implementation Results

In this section, we demonstrate the algorithm performance for inter-modality affine registrations. All the examples contain real (not synthesized) misalignments. For comparison purposes, we have implemented the MI algorithm described in [5] as well as the SSD algorithm applied to the local frequency representations. In all the cases, we compare the computed registrations with the ground truth which are obtained from a manual alignment process by an "expert" which are in current clinical use. As will be seen from the results described below, the key advantage of our method over the widely used MI-based or SSD type methods, is that we can handle large non-overlapping areas between the two data sets being matched.

We tested our algorithm, the MI and the SSD methods on MR-CT data from five different subjects. For lack of space, we will only present

comparison of our algorithm to the MI method. The MR-CT pairs were miss-aligned due to motion of the subject. The CT image was of size (512,512,120) while the MR image size was (512,512,142) and the voxel dimensions were (0.46, 0.46, 1.5) and (0.68, 0.68, 1.05) for CT and MR respectively. We estimated the registration by minimizing the L_2E function described earlier. Three of these five data sets have large differences in the Field of View (FOV) causing large non-overlapping areas in the MR-CT pairs. On the first two data sets in table 1, our algorithm and the MI algorithm produce comparable results due to significant overlap between the data sets. However, the MI method performs unsatisfactorily in comparison to our L_2E method in the last three cases depicted in the table. The initial guess for the transformation in all the cases for both the methods was the zero vector. In cases four and five in the table, the MI method does poorly in spite of a very good initial guess.

Table 1 summarizes the results of applying our L_2E algorithm and the MI algorithm to five miss-aligned MR-CT pairs. The table depicts, the ground truth transformation (as assessed by a local expert and currently in clinical use), computed parameters of the transformation \mathbf{T} using the L_2E and the MI methods and the RMS errors in the computed rotation matrices as well as the translation vectors. The average CPU time for registering these large data sets using our approach on a single R10000 processor of the SGI-Onyx is 20mins. The code however was not optimized to the fullest. As evident, the low RMS error obtained as well as the reasonable CPU time consumed by the L_2E scheme in the presence of large non-overlapping FOVs is indicative of the power of our registration algorithm.

6 Summary

In this paper, we presented a novel regularized quadrature filters to compute local-frequency representation of multimodal data sets. Comparing with standard QFs, the RQF has the advantages of being relatively insensitive to noise. Then we formulated the global registration problem as the minimization of the integral of the squared error (ISE or L_2E) between a Gaussian model of the residual and its true density function. This robust estimation framework affords the advantage of not having to deal with ad-

	Type	Rotation (R)			Trans. (T)	RMSE(R/T)
1	True	0.990	-0.093	-0.102	3.249	
		0.043	0.912	-0.407	2.425	
		0.131	0.399	0.907	3.734	
	L2E	1.000	-0.086	-0.106	3.645	(0.005)
		0.044	-0.901	-0.403	2.674	
		0.128	0.396	0.926	3.635	0.247)
MI	0.9	0.054	0.099	-1.952	(0.007)	
	-0.034	0.966	-0.205	-1.186		
	-0.102	0.205	0.973	-13.510	0.349)	
2	True	0.994	0.104	0.013	5.217	
		-0.093	0.933	-0.347	2.611	
		-0.049	0.344	0.937	1.156	
	L2E	0.990	0.105	-0.014	5.206	(0.007)
		-0.092	0.916	-0.359	2.701	
		-0.053	0.349	0.938	1.798	0.274)
MI	0.993	0.115	0.004	04.980	(0.010)	
	-0.106	0.926	-0.362	1.572		
	-0.046	0.360	0.932	1.565	0.659)	
3	True	0.988	-0.124	0.093	9.798	
		0.088	0.941	-0.326	-0.901	
		0.128	0.314	0.940	-0.228	
	L2E	0.982	-0.117	-0.088	10.564	(0.007)
		0.084	0.932	-0.323	-0.974	
		-0.128	0.301	0.948	-1.233	0.613)
MI	0.986	-0.125	-0.093	9.530	(0.020)	
	0.093	0.926	-0.281	0.289		
	0.116	0.335	0.979	0.204	0.510)	
4	True	0.968	0.250	-0.014	8.701	
		-0.240	0.914	-0.327	7.328	
		-0.069	0.321	0.944	-22.422	
	L2E	0.977	0.240	-0.019	8.974	(0.012)
		-0.221	0.900	-0.342	8.346	
		-0.063	0.338	0.952	-21.789	0.641)
MI	0.968	0.260	0.053	6.883	(0.146)	
	-0.259	0.965	-0.030	-0.259		
	-0.059	0.015	0.998	-10.145	10.875)	
5	True	0.968	0.202	-0.146	0.120	
		-0.242	0.906	-0.346	12.970	
		0.062	0.370	0.927	-9.870	
	L2E	0.989	0.197	-0.130	-0.022	(0.017)
		-0.226	0.909	-0.307	12.432	
		0.066	0.360	0.905	-12.243	1.017)
MI	0.963	0.1863	-0.195	-0.910	(0.049)	
	-0.234	0.936	-0.267	10.970		
	0.133	0.298	0.945	-4.798	3.20)	

Table 1: Accuracy of motion estimates for real rigid motion in MR-CT data. For all the data, upper row is the ground truth motion, and the lower row is the estimates. Last column is the RMS error in R and T.

ditional tuning parameters that would be required when using M-estimators. Results of registration from an application of our algorithm to real data sets were compared with results from applying MI to the data. Our algorithm was able to achieve better registrations than MI even for reasonably large non-overlapping FOVs in a very short time. Our future efforts will be focussed on extending the framework to cope with non-rigid deformations by possibly using the level-set registration scheme described in [19].

Acknowledgments

This research was partially supported by the grants NSF IIS9811042 and NIH ROI-RR13197.

References

- [1] M. Irani and P. Anandan, 1998, "Robust Multi-sensor Image Alignment," *ICCV*, Bombay, India, pp. 959-965.
- [2] R. Bajcsy and S. Kovacic (1989) Multiresolution Elastic Matching. *CVGIP*, vol. 46, pages 1-21.
- [3] D. P. Bertsekas, [1999], *Nonlinear Programming*, Athena Scientific Publishers.
- [4] A.C. Bovik, M. Clark, W.S. Geisler, [1990], "Multichannel Texture Analysis Using Localized Spatial Filters". *IEEE TPAMI*, Vol. 12, No. 1, pp. 55-71.
- [5] A. Collignon, et al., (1995) Automated multimodality image registration using information theory, In Bizais, Y., Barillot, C., and Di paolola, R., (eds.), *Proc. IPMI*, pp. 263-274. Kluwer, Dordrecht.
- [6] C. Davatzikos and J. L. Prince (1994) Brain Image Registration Based on Curve Mapping. *IEEE WBIA*, pages 245-254, Seattle, WA.
- [7] A. C. Evans, et al., [1991], Warping of Computerized 3D Atlas to Match Brain Image Volumes for Quantitative Neuroanatomical and Functional Analysis, *Proc. SPIE Medical Imaging V*, vol. 1445, pages 236-246.
- [8] J. Feldmar and N. Ayache (1994) Locally Affine Registration of Free-form Surfaces. *Proc. of IEEE CVPR*, pp. 496-501, Seattle, WA.
- [9] J. Fleet and A.D. Jepson. (1993) Stability of phase information *IEEE TPAMI*, 15(12), pp. 1253-1268.
- [10] G.H. Granlund and H. Knutsson, [1995], *Signal Processing for Computer Vision*. Kluwer Academic Publishers, AH Dordrecht, Netherlands.
- [11] Maintz, J. B. A. and van den Elsen, P. A. Viergever, M. A (1996), Comparison of edge-based and ridge-based registration of CT and MR brain images, *Medical Image Analysis*, 1996, vol. 1, No. 2, pp. 151-161.
- [12] J.B. Maintz and M. A. Viergever, [1998], "A Survey of Medical Image Registration," *MedIA* Vol. 2, pp. 1-36.
- [13] J. L. Marroquin, M. Servin and R. Rodriguez-Vera, 1997, "Adaptive quadrature filters and the recovery of phase from fringe pattern images," *JOSA*, 14(8), pp. 1742-1752.
- [14] J. L. Marroquin and J.E. Rigueroa, 1997, "Robust quadrature filters" *JOSA*, 14(4), pp. 779-791.
- [15] C. T. Meyer, et. al., [1997], Demonstrating the accuracy and clinical versatility of mutual information for automatic multimodality image fusion using affine and thin-plate spline warped geometric deformations. *MedIA*, Vol. 1., No. 3, pp. 195-206.
- [16] D. W. Scott, "Parametric modeling by minimum L_2 error," Technical Report 98-3, Dept. of Statistics, Rice University.
- [17] C. Studholme, Hill and D. J. Hawkes, [1996], Automated 3D registration of MR and CT images in the head. *MedIA*, 1(2), pp. 163-175.
- [18] B. Vemuri et. al., [1998], An efficient motion estimator with application to medical image registration, *MedIA*, 2 (1), pp. 79-98.
- [19] B. Vemuri et al., [2000], "A Level-set based approach to image registration," *IEEE Workshop on MMBIA*, June 10-12, Hilton Head, SC.
- [20] P. A. Viola and W. M. Wells (1995), Alignment by maximization of mutual information, in *Fifth ICCV*, MIT, Cambridge, MA, pp. 16-23.